Chapter-6

Studies the optical and dielectric behaviour of Hexagonal Plate like ZnO nanoceramic

6.1Introduction

Hexagonal structures of ZnO are made up of several closely packed and randomly aligned nano-crystallites. It has considerably attracted important material due to its unique morphology dimension-dependent optoelectronic properties (Y.Nakayama, et al. 2007). In recent, Zinc oxide is referred to as a direct bandgap I-VI semiconductor compound with a band gap about 3.30 eV and large exciting binding energy of about 6meV (S.H.Yu, et al.2002). It has special properties, such as high chemical activity and novel optical, mechanical, electromagnetic, etc. and wide commercially application (R.Yadav et al.2019; A.K. Baral, et al.2019). In previous studies, there are several reports on the synthesis of nanoplate-like ZnO nanoparticles parties (S.Sucharitakul et al.2018). However, most of these reports are concerned with different structures with toxic capping reagent or expensive substrates. Thus, there is a need to develop a method for the preparation of hexagonal plates shaped structure that avoids toxic capping reagents and substrates. For this, the hexagonal plates shaped of ZnO is of great interested and have many advantages due to its highly polar surfaces area (E.S.Jang, et al.2017). These many approaches have been employed to the fabrication of special morphological of ZnO nanostructures. There are different methods have been used for the production of ZnO nanoparticles such as chemical synthesis, hydrothermal method, electrophoresis deposition, co-precipitation, mechanochemical thermal synthesis, chemical vapor depositions (F. Zahra,et al.2013). Among all methods, precipitation and sol-gel technique provide

suitable control of nucleation, and growth of particles in solution. Sol-gel technique is also one of the simple and cost-effective methods for bulk production of materials (L.Wang L.et al.1999). The synthesis of size and shape controlled nanoparticles and their assembly into materials still poses a challenge in the area of nanoscience. It is well recognized that the shape of the nanoparticle plays a crucial role in determining their resultant properties (S.H.Yu, et al.2002; J.Yang, et al. 2002; Y.T.Chem, et al.2003; A.P.A. Oliveira, et al.2003). Factors such as concentration, temperature, temperature, pH, capping agent and the reaction time are critical parameters that influence the size and the morphology of the nanoparticles. Among these factors, the temperature is also important for altering a synthesis strategy can also introduce surprising results because of heat treatment affect the semiconductor host lattice (F.L.Xian et al. 2012). The annealing temperature is impartment parameters which are effect the morphology of the synthesis materials (S.Sucharitakul,et al.2018).

Keeping the above-mentioned facts, the objective of the present work was to obtain a particular structure of ZnO. We have been synthesized this particular structure of ZnO by sole-gel method and obtain hexagonal plate shape zinc oxide structures. Therefore, our synthesis approaches provide a simple, cost-effective easily and convenient route to obtain largely quantizes of hexagonal plate shape zinc oxide structures. The effect of annealing temperature on the synthesized hexagonal plate shape ZnO was also investigated. Moreover, the optical and dielectric properties had also been studies. The results showed that with increasing annealing temperature the morphology of ZnO altered and forming porous feature at the higher temperature. The effect of annealing temperature on the synthesized hexagonal plate shape ZnO and its optical and dielectric behavior were also observed.

6.2 Results and Discussion

6.2.1 Reaction mechanism

During the formation process of ZnO the growth process of ZnO crystalline grains was obtained by nucleation and growth. The specific reaction process described as reactants $ZnSO_4.7H_2O$ was hydrolyzed quickly with the increasing of temperature under hydrothermal conditions, resulting it gets converted into zinc sulfate and water by thermal decomposition (Straszko J. et al.1997) according to reaction (6.1-6.3). It gets further converted into $[Zn\ (NH_3)_4]^{2+}$ during zinc ammonia complex reaction with diluted ammonia solution. In our case, four hydroxyl ions of ammonia react with the Zn^{2+} and form building blocks of zinc ammonia complex reaction $[Zn(NH_3)_4]^{2+}$ and when the temperature increases, the four coordinated complex ions changes to ZnO, ammonia and water molecules. It is assumed that the initially formed $[Zn\ (NH_3)_4]^{2+}$and $[Zn\ (OH)_2]$ according to reaction (6.4),(6.7). It gets aggregated after acquiring sufficient thermal energy in the solution. The transformation from zinc complex ion $[Zn\ (NH_3)_4]^{2+}$ to ZnO is a kinetic-controlled growth process at this state in the solution. Increasing the temperature of the solution it will form Zn^{2+} and OH^- and will lead to rapid nucleation, and then form active ZnO nuclei according to reaction (6.9).The active ZnO nuclei thus formed are expected to be the building blocks for the formation of the final product. The active molecules are generally referred to as primary stems and form in hexagonal plate-shaped. The remaining growth units directionally grew around the ZnO nuclei, and formed ZnO nanostructures, according to reaction (6.10). The process of formation of ZnO hexagonal powders can be represented by the following equations.

$$ZnSO_4.7H_2O \rightarrow ZnSO_4.6H_2O + H_2O \text{---------- (6.1)}$$

$$ZnSO_4.6H_2O \rightarrow ZnSO_4.H_2O + 5H_2O \text{---------- (6.2)}$$

$$ZnSO_4.H_2O \rightarrow ZnSO_4 + H_2O \text{---------- (6.3)}$$

$$ZnSO_4 + 4NH_3 \rightarrow [Zn(NH_3)_4]^{2+} \text{---------- (6.4)}$$

$$H_2O \rightarrow H^+ + OH^- \text{---------- (6.5)}$$

$$2OH^- + [Zn(NH_3)_4]^{2+} \rightarrow ZnO + 4NH_3 + H_2O \text{---------- (6.6)}$$

$$[Zn(NH_3)_4]^{2+} + H_2O \rightarrow Zn(OH)_2 + 3NH_4OH \text{---------- (6.7)}$$

$$Zn(OH)_2 \xrightarrow{temperature} Zn^{2+} + 2OH^- \text{---------- (6.8)}$$

$$Zn^{2+} + 2OH^- \rightarrow ZnO\ (nuclei) + H_2O \text{---------- (6.9)}$$

$$Zn^{2+} + 4OH^- \rightarrow Zn(OH)_4^{2-} \text{---------- (6.10)}$$

$$Zn(OH)_4^{2-} \rightarrow ZnO + H_2O + 4OH^- \text{---------- (6.11)}$$

ZnO crystalline grains were obtained by nucleation and growth of ZnO nuclei. In the reaction mechanism $ZnSO_4.7H_2O$ was hydrolysed with increasing of the temperature resulting it gets converted into zinc sulphate and water by thermal decomposition (J. Straszko et al.1997) according to reaction (6.12-6.14). In diluted ammonia, zinc ammonia complex $[Zn(NH_3)_4]^{2+}$ reaction is formed. In reaction, four hydroxyl ions of ammonia react with the Zn^{2+} and form building blocks of $[Zn(NH_3)_4]^{2+}$. It is assumed that the initially formed $[Zn(NH_3)_4]^{2+}$ and $[Zn(OH)_2]$ according to reaction (6.15) and (6.17). It gets aggregated after acquiring sufficient thermal energy in the solution. It gets aggregated after acquiring sufficient thermal energy in the solution. The transformation from $[Zn(NH_3)_4]^{2+}$ to ZnO is a kinetic controlled growth process. Increasing the temperature of the solution it will form Zn^{2+} and OH^- and then form active ZnO nuclei according to reaction (6.19).The

active ZnO nuclei thus formed building blocks of hexagonal plate shaped, according to reaction (6.22). The process of formation of ZnO hexagonal powders can be represented by the following equations.

$$ZnSO_4.7H_2O \rightarrow ZnSO_4.6H_2O+H_2O \text{---------- (6.12)}$$

$$ZnSO_4.6H_2O \rightarrow ZnSO_4.H_2O +5H_2O \text{---------- (6.13)}$$

$$ZnSO_4.H_2O \rightarrow ZnSO_4+H_2O \text{---------- (6.14)}$$

$$ZnSO_4 +4NH_3 \rightarrow [Zn\ (NH_3)_4]^{2+} \text{---------- (6.15)}$$

$$H_2O \rightarrow\ H^+ + OH^- \text{---------- (6.16)}$$

$$2OH^- + [Zn\ (NH_3)_4]^{2+} \rightarrow ZnO + 4NH_3 + H_2O \text{---------- (6.17)}$$

$$[Zn\ (NH_3)_4]^{2+} + H_2O \rightarrow Zn\ (OH)_2 + 3NH_4OH \text{---------- (6.18)}$$

$$Zn\ (OH)_2 \xrightarrow{temperature} Zn^{2+} + 2OH^- \text{---------- (6.19)}$$

$$Zn^{2+} + 2OH^- \rightarrow ZnO\ (nuclei) + H_2O \text{---------- (6.20)}$$

$$Zn^{2+} + 4OH^- \rightarrow Zn\ (OH)_4^{2-} \text{---------- (6.21)}$$

$$Zn\ (OH)_4^{2-} \rightarrow ZnO + H_2O + 4OH^- \text{---------- (6.22)}$$

6.2.2 Characterizations of Materials

Hexagonal plate-like ZnO was synthesis by using the sol-gel method. The synthesis method of Hexagonal plate-like ZnO has been discussed in chapter-3 (**section-3.4.4).**The samples of Hexagonal plate-like ZnO were annealing at temperature 700^0C, 900^0C and 1100^0C on the sample with a constant heating rate. The synthesized samples were coded by ZnO, ZnO700^0C, ZnO900^0C and ZnO1100^0C. XRD patterns of ZnO at different annealing temperatures are shown in figure 6.1 (a). From this figure, all reflection planes were calculated at diffraction angle. Reflection planes have been mached with the standard JCPDS card no 36-

1451(in appendix-2) for all sample and listed in appendix-12 to 15. The observed diffraction corresponding to reflection plane (100), (002), (101), (102), (110), (103), (200) (112) (201), (004) and (202) provides a clear evidence for the formation of a single phase wurtzite ZnO structure (JCPDS36-1451) (F.Gu et al.2004). It is also observed diffraction peaks in the sample ZnO and ZnO700 ^{0}C towards lower Bragg's angle (2θ=30°) also appears. Reflection planes have been mached with the standard JCPDS card no 25-1029(in appendix-2) for the sample ZnO and ZnO700 and listed in appendix-16&17 which are represent zinc oxalate reflection peak. It is disappear in the sample ZnO900^{0}C and ZnO1100^{0}C which indicates samples contain zinc oxalate like impurities during the synthesis and annealing at temperature>700^{0}C remove the impurities and exhibit sharp peaks indicating that all samples were highly crystalline. The peak intensities of ZnO increase gradually and get sharpened with increasing annealing temperature indicating that the crystalline nature of ZnO particles. It is also observed from XRD spectra annealing behavior also influence the structural properties. The figure 6.1 (b) and inset of figure 6.1 (b) shows the relative intensity increase for the peaks corresponding to the (002) with increasing annealing temperature. The enhanced intensity of all samples is indicating preferred orientation along c-axis. Other peaks of weak intensity in this curve can be ascribed to its poor crystalline. Figure 6.1(c) shows the crystallite size which is estimated by employing eqn(3.7). The average crystallite size was found to be 30nm, 16nm, 40nm, and 45nm for the sample ZnO, ZnO700^{0}C, ZnO900^{0}C, and ZnO1100^{0}C respectively which is also listed in table 6.1. It is observed that the average crystallite size of the sample ZnO700^{0}C decreases where're sample ZnO900^{0}C, ZnO1100^{0}C increase which indicates the temperature affect the growth of ZnO nanoparticles. It is observed that

the structures of the ZnO prepared under the different annealing temperature are the same phase although they have different morphology. Thus, the change in the morphology of the samples does not alter the crystalline phases.

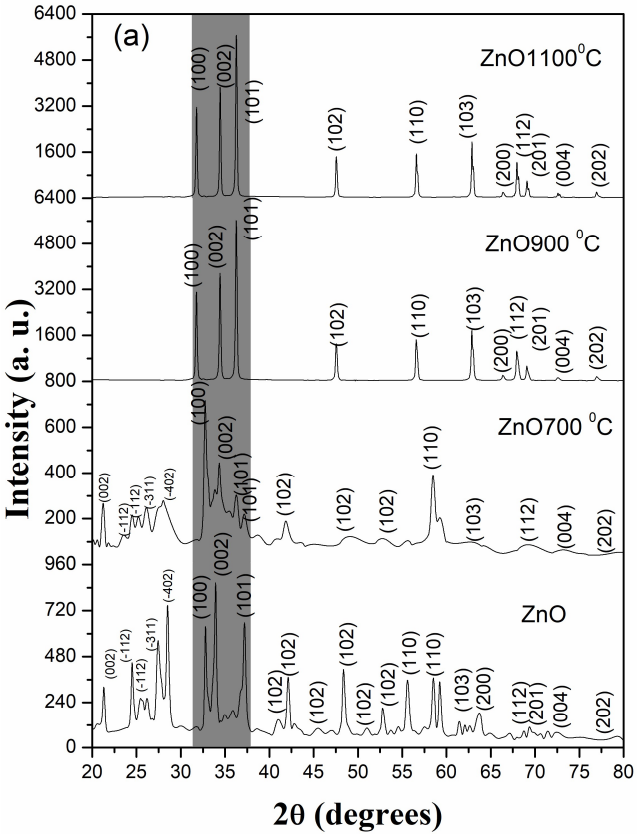

Figure 6.1 (a) XRD pattern of sol-gel derived ZnO powder and their annealing at different temperature.

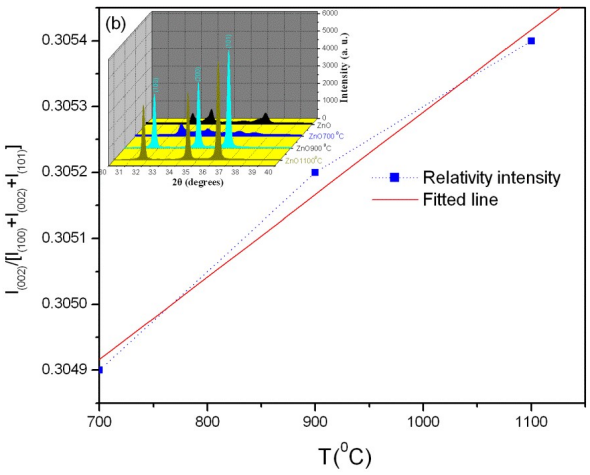

Figure 6.1 (b) The relative intensity of (002) peaks vs. annealing at different temperature.

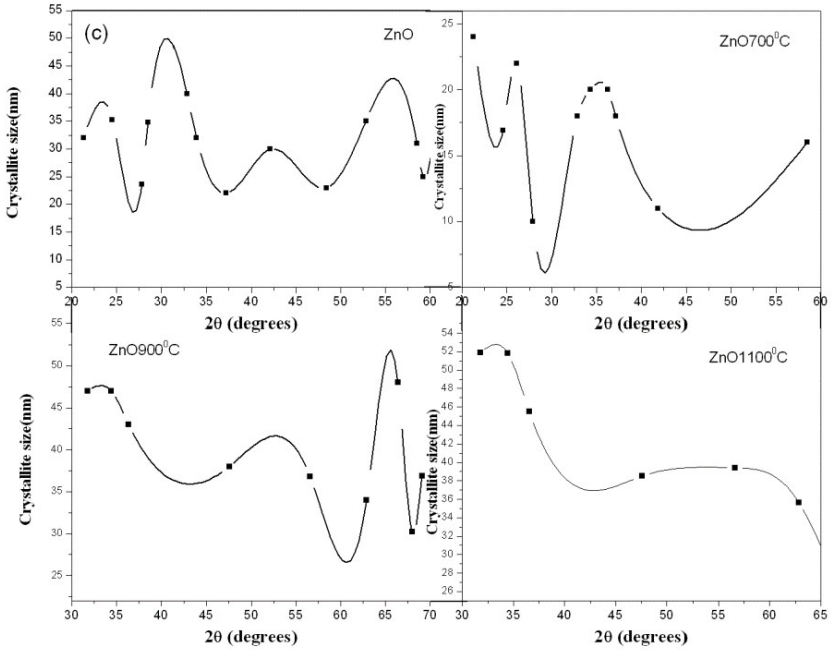

Figure 6.1 (c) The variation of crystalline size of ZnO, ZnO700^{0}C, ZnO900^{0}C and ZnO1100^{0}C.

Table 6.1 Lattice parameters of ZnO prepared at annealing temperatures of 700^{0}C, 900^{0}C, 1100^{0}C.

Sample	Grw. Tem.	parameters **a± σ [A^0]** (100)	c ± σ [A^0] (002)	Cryst. size(nm) (101)	ε_{xx}%	ε_{zz}%	Structure	E_g (eV)
ZnO	RT	3.15192 ±0.098	5.28773±0.080	30	-3.25	1.55041	Hexagonal plate	3.21
ZnO700	700	3.22929 ±0.020	5.22566±0.018	16	-0.6372	0.35836	rods and disk	3.25
ZnO900	900	3.43917±0.18	5.16726±0.039	40	-5.82061	-0.7632	porous	3.22
ZnO1100	1100	3.25067±0.0006	5.20658±0.0004	45	0.02062	-0.019	Grainual	3.14
card		3.250	5.207					

6.2.3 Strain/Stress behavior of Hexagonal plate by X-ray profile analysis

Figure 6.2 shows the shadow region of the figure 6.1(a) in which, peak of the plane (100) is 1° shifted toward the lower degree, peak of the plane (002) is 0.51° shifted toward the higher degree and peak of the plane (101) is 0.93° shifted toward the lower degree . These peaks are shifted as like lower -higher-lower degree shifted as compared to the ZnO peaks. These types of shifting behaviors are seen in whole XRD spectrum. This type of variation could be explained by schematics representation of unsrained, uniform tensile strain and nonuniform strain which are shown in figure 6.3(a-c). The uniform strain affect the peak position and the nonuniform strain affect the peak broadening and intensity. The effect of strain, both uniform and nonuniform, on the direction of X-ray reflection is illustrated in 6.3(a-c). A portion of an unstrained grain appears in panel (a) on the left, and set of transverse reflecting planes shown has a uniform equilibrium spacing d. The diffraction line from these planes appears on the right. If a uniform tensile strain is applied to a grain at right angles to the reflecting planes, their spacing becomes larger than d and the corresponding diffraction line shifts to lower angles but does not otherwise changes as shown in panel(b).This line shift is the basis of the X-ray method for the measurement of microstress. In (c) the grain is bent and the strain is nonuniform; on the top (tension) side the plane spacing exceeds d, whereas on the bottom (compression) side it is less than d, and some where in between it equals d_o (N.S.Ramgir et al. 2006). However, the peak width derived from crystallite size varies as $1/\cos\theta$, where as strain varies as $\tan\theta$. This difference in behavior as a function of 2θ enables one to discriminate between them and strain effects on peak broadening. The Bragg width contribution from crystallite size is inversely

proportional to the crystallite size (V.K. Pecharsky, et al.2003).

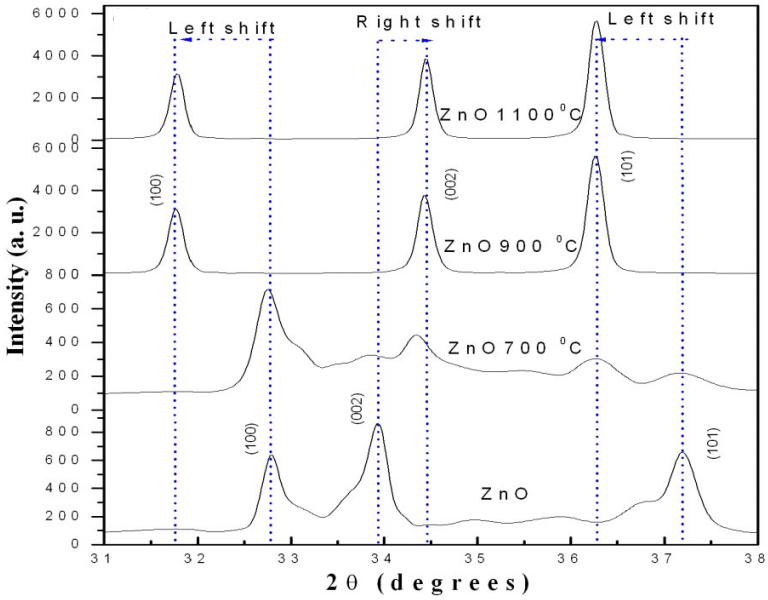

Figure 6.2 XRD pattern of shifting in peaks position of (100), (002) and (101) of ZnO, ZnO700^{0}C, ZnO900^{0}C and ZnO1100^{0}C.

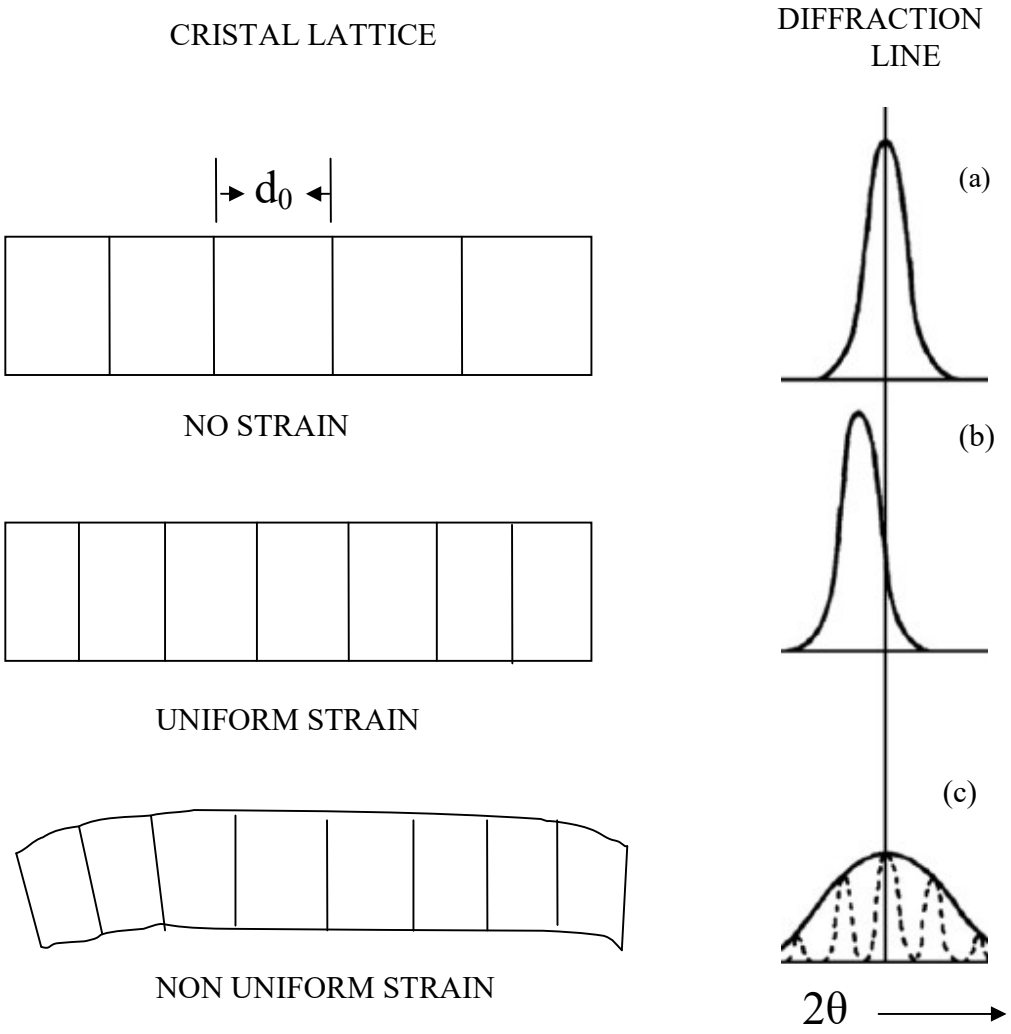

Figure 6.3 Schematics representation of Unsrained, Uniform tensile strain and nonuniform strain.

Figure 6.4 (a) shows the variation of lattice constant "a" and "c"of the plane (100), (002) with various growth temperatures which are evaluated from the XRD data and estimated error bars (±σ) also listed in table 6.1. The lattice parameters was constant "a" of the plane (100) increase up to 900^0C and then decrease and the lattice constant "c" of the plane (002) decrease up to 900^0C and then increase. It is observed that decreasing and increasing of lattice constants due to the effect of annealing

temperature and variation of morphology. The Figure 6.4 (b) shows the variation of full-width half maxima (FWHM) with an annealing temperature of the plane (100) (002) and (101). It is observed FWHM is decreased with increasing the annealing temperature. On the basis of the above data gathered their mechanism of shifting, the variation of lattice parameters and FWHM for the XRD peaks. These could become an interesting issue. So a degree of shifting, the variation of lattice parameters and FWHM indicating that there is an internal strain in the lattice due to the lattice mismatch of ZnO interlayer. For crystals of hexagonal structure, the lattice parameters are related to each other such as a=b=c, $\alpha = \beta = 90^{O}, \gamma = 120^{O}$ and "a" and "c" are given by eqn. (3.9) according to the (100) and (002) plane orientation respectively. First, we calculated the lattice parameters from the X-ray diffraction data then calculated the value of strain along the a-axis (ε_{xx}) in the plane and normal-to-the plane along c-axis (ε_{zz}) by eqn. (3.17&3.19) under the influence of biaxial and isotropic modal. The lattice parameters of ZnO, annealed at different annealing temperatures, yield a hexagonal unit cell which is very close to the parameters of a_0= 3.250 A° and c_0=5.270 A° (JCPDS 36-1451). The strain along c-axis (ε_{zz}) calculated by eqn.(3.22).The calculated results based on the values of inter-planar distance d_{100} and d_{002} and *hkl* dependent strains and lattice parameters are tabulated in table 6.1. For the sample grown at room temperature the lattice parameters were larger than the known bulk value of 5.270A^0 and lower at temperature 700^{0}C which indicates that the unit cell is elongated along the c-axis for the sample grown at 900^{0}C and 1100^{0}C, the lattice parameters of the ZnO decrease.It is also observed from the table 6.1 that the value of ε_{xx} for the sample ZnO and ZnO700 is negative (compressive) and value

of ε_{zz} is positive (tensile). However, the value of ε_{xx} for the sample ZnO900 and ZnO1100 is positive (tensile) and value of ε_{zz} is negative (compressive).These variations in the lattice parameter clearly show that the residual stress can be relaxed upon high growth temperature. These behaviors are also shown in figure 6.4 (c) and (d). From the data in table 6.1, it is also observed that grain size and strain effected with annealing temperatures. The crystalline particles of ZnO agglomerated to each other with increasing the annealing temperature and form grain. The grain size was calculated by eqn. (3.7) on the diffraction peak corresponding to the plane (101). Figure 6.4 (c) and (d) shows the grain size and strain along the a-axis and c-axis at different annealing temperatures. In figure 6.4 (c) grain size increase and strain decrease with increasing annealing temperature and in figure6.4(d) grain size increase and strain decrease at 900^0C and further the increase with increasing annealing temperature. Due to the increase in grain size, the density of grain boundaries at higher temperature is smaller than that grown at low temperatures. Figure6.4 (e) shows the variation of FWHM and grain size against the stress values of the (002) peak. FWHM decreases with increasing compressive stress and increases with increasing tensile strength, which may be due to the grain growth and improvement in crystallinity. According to previous studies, the residual stress reduction is consequently accompanied by an improvement in crystallinity, which is manifested by the large grain size (Lee Y.C. et al. 2009; V.Gupta, et al.1996; M.K.Puchertet al.1996). Figure 6.4 (f) shows the stress-strain plot at different annealing temperature in which it shows the linear relation and from this relation, Young modulus could be calculated from the slope of the graph. The Hookes's law

referrers to the strain and there is a linear proportionality between the stress and strain as given by $\sigma = \varepsilon Y_{hkl}$, or $\varepsilon = \sigma / Y_{hkl}$ where σ is stress of the crystal ε is anisotropic microstrain, this will depend on the crystallographic direction and Y_{hkl} is the modulus of elasticity or Youngs modulus. The elastic compliances of ZnO calculated by equation (3.25) with values 7.8589×10^{-12}, $-2.206 \times 10^{-12,}$ 6.9409×10^{-12}, and 23.579×10^{-12} m^2N^{-1} respectably (J.F. Nye 1985). Young's modulus Y_{hkl} for hexagonal ZnO nonparties was calculated as ~129 GPa.

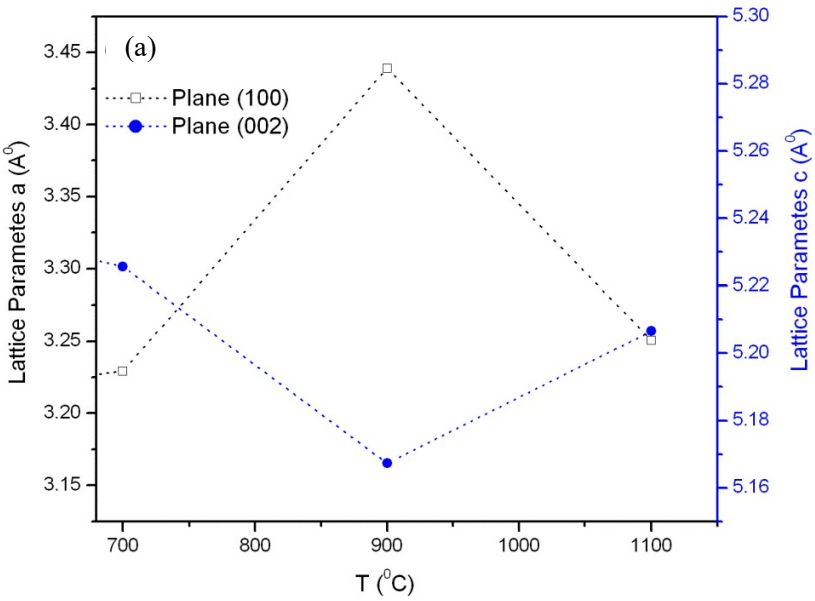

Figure 6.4 (a) Variation of lattice constant a and c of the plane (100) and (002) with different annealing temperature.

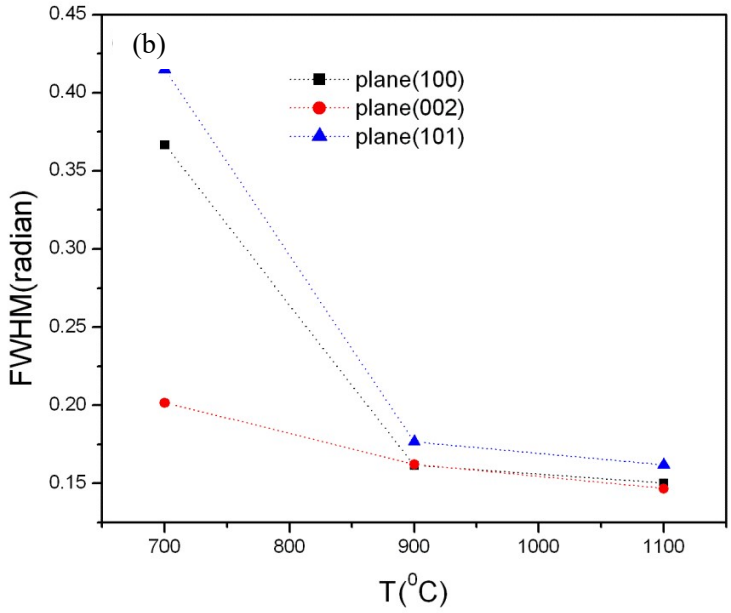

Figure 6.4 (b) Variation of FWHM of the plane (100) (002) and (101) with different annealing temperature.

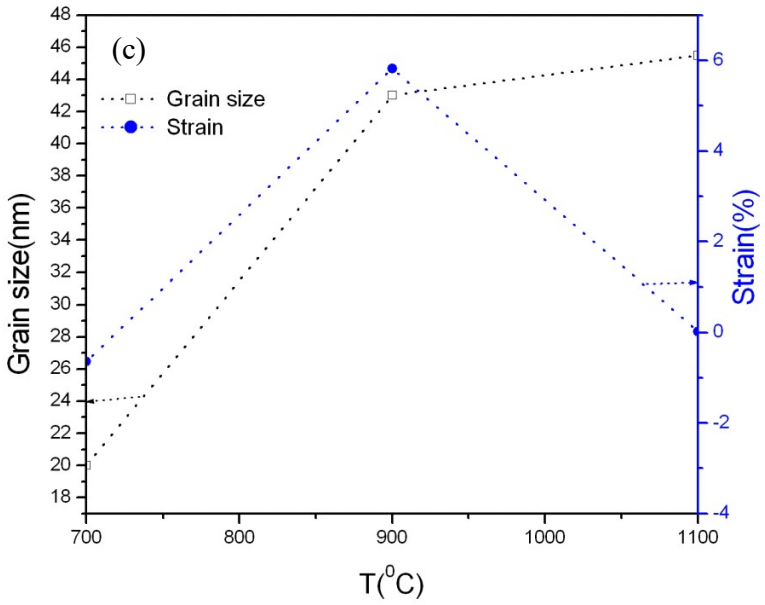

Figure 6.4 (c) Variation of grain size and strain of the plane (100) with different annealing temperature.

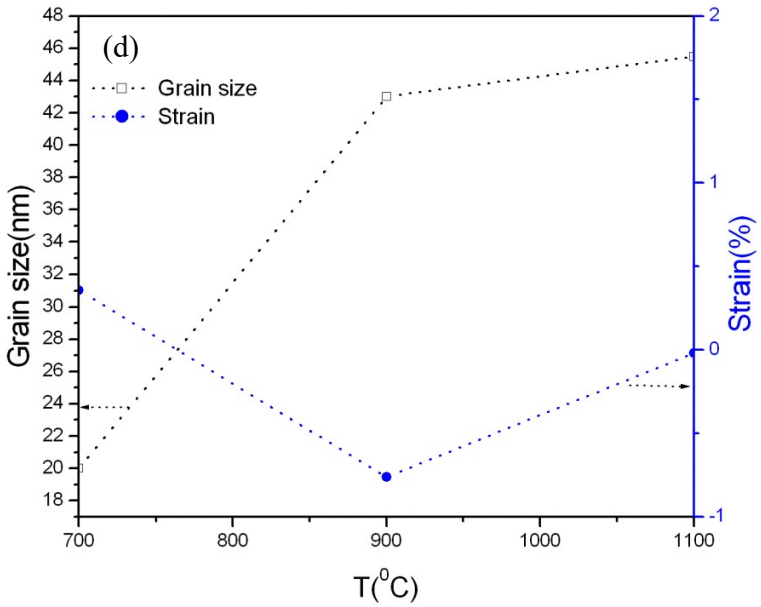

Figure 6.4 (d) variation of grain size and strain of the plane (002) with different annealing temperature.

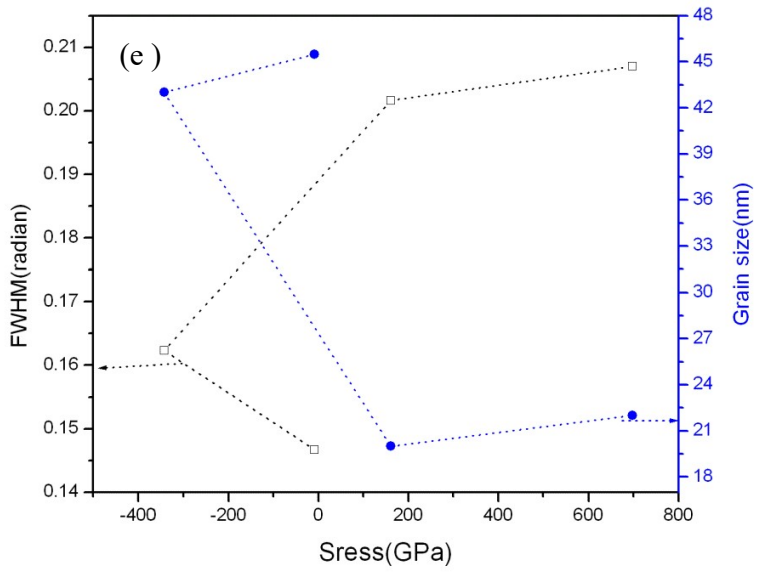

Figure 6.4 (e) Variation of FWHM and grain size with stress of ZnO700^{0}C, ZnO900^{0}C and ZnO1100^{0}C.

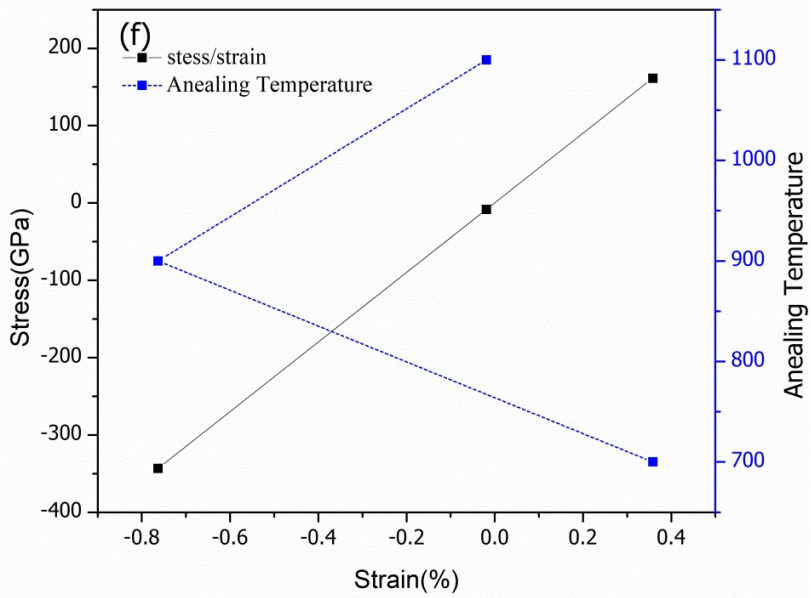

Figure 6.4 (f) Stress and stain plot of hexagonal plates at different annealing temperature.

6.2.4 Williamson-Hall analysis

Williamson-Hall X-ray liner broadening analysis provides a method of finding an average size of coherently diffracting domains and strains. Strain-induced peak broadening arises due to crystal imperfection, which has been calculated using the relation eqn. (3.24). The equation (3.24) represents the linear plot of $\beta_{hkl}\cos\theta$ against 4sinθ. From the linear plot of $\beta_{hkl}\cos\theta$ against $4\sin\theta$, we are able to calculate the strain as well as the crystallite size of the samples. In principle, the slope of the graph gives the strain, whereas the reciprocal of the intercept should be the crystallite size (L.Wang, et al.1999).

Figure 6.5(a-d) represents the W-H plot of the samples ZnO, ZnO700^{0}C, ZnO900^{0}C, and ZnO1100^{0}C respectively. A positive and negative strain of the ZnO, ZnO700^{0}C, ZnO900^{0}C, and ZnO1100^{0}C are tabulated in table 6.1 and similar to

observed strain from the figure 6.4 (c) and figure 6.4(d). A negative strain of ZnO, ZnO700^{0}C, and ZnO900^{0}C around the value 2.64498 x 10^{-4}, 2.52398 x 10^{-4} and at 5.18x10^{-4} was observed from the slope of figure 6.5(a-c) respectively. It is also observed positive strain of the sample ZnO1100^{0}C around the value 4.88x10^{-4}.It is observed from the table 6.1 that with the increasing annealing temperature from 700 to 1100 the strain associated with the samples decreased with a gradually increase in crystallite size. Although X-ray profile analysis is an averaging method, apart from TEM imaging it still holds a dominant position in grain-size determination.

The crystallite size calculated from the intercept of the samples ZnO, ZnO700^{0}C, ZnO900^{0}C, and ZnO1100^{0}C is 29nm, 17nm, 41nm, and 46nm respectively, which is also approximately similar to the calculated by Debye-Scherer'sequation (3.7). Figure 6.5(e) shows dislocation density versus temperature which is obtained by using the equation (3.11). It is observed that dislocation density decrease with increasing the annealing temperatures which suggested an increasing the crystallinity of ZnO.

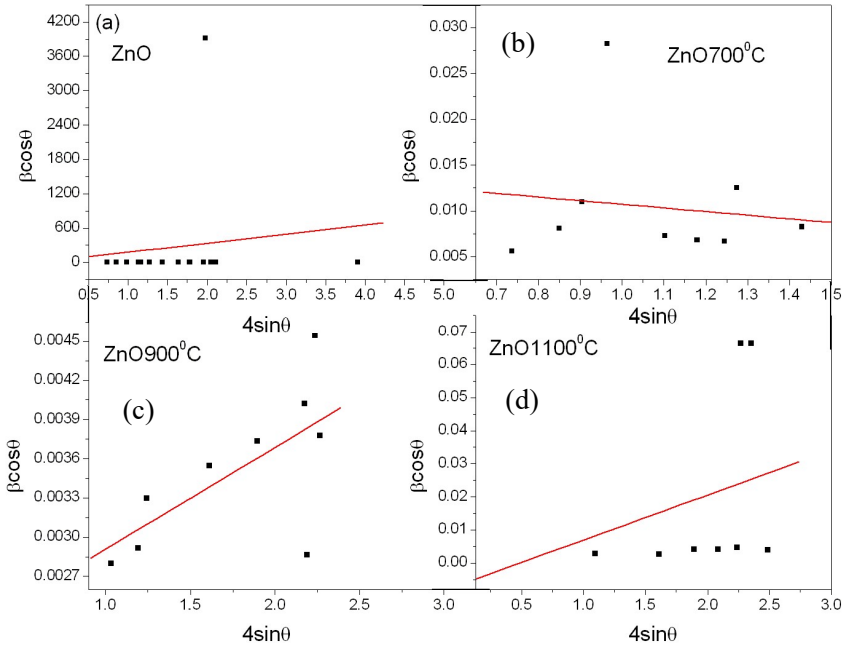

Figure 6.5 Williamson-Hall analysis's of (a) ZnO, (b) ZnO700 ^{0}C, (c) ZnO900 ^{0}C and (d) ZnO1100 ^{0}C.

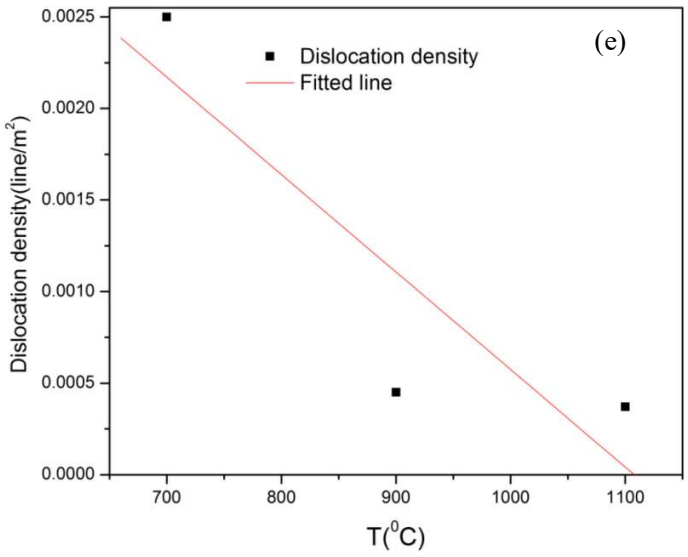

Figure 6.5 (e) variation of dislocation density at the different annealing temperature.

6.2.5 Morphological analysis

From the figure 6.6 (a) the structure of the prepared sample is in hexagonal morphology. In order to elucidate the effect of annealing temperature on this structure the sample was annealed at ZnO700^{0}C, ZnO900^{0}C, and ZnO1100^{0}C. It was indicated from figure 6.6 [(b)-(d)] the annealing temperatures have a significant impact on the ZnO morphological structure. Figure 6.6 (b) shows the annealing of the hexagonal plate at 700^{0}C it is improving the orientation degree and the morphological structure was converted into rods and disks like structure having an average diameter in the micron range. This conversion may be regarded as the annealing process of ZnO that enhances the grain-growth rate and increases the densification behavior of the materials that yield the rod and disk-like microstructure. Another region when annealing temperature increase as a result of excessive oxygen molecules present in the surface structure. The trapped oxygen molecules located in the empty site between interconnected structures made ZnO disks and split into rods like structures. Figure 6.6(c) shows increasing magnification micrograph at temperature 900^{0}C. At this temperature can be observed the hexagonal morphology of ZnO tends to form a many porous like structure. However, when the annealing temperature increase at 1100^{0}C the porous like structure disappears that may break down the pore boundaries to yield grain like the site that is suitable for ZnO growth and this is aggregated to form grain-like structure. The increasing magnification micrograph at 1100^{0}C is shown in figure 6.6 (d). In generals for the ZnO, there are many dangling bonds related to the zinc and oxygen defects at grain boundaries. As a result, these defects are favorable for the merging process to form large ZnO grain when increasing annealing temperature. A typical EDX spectroscopy of ZnO,

ZnO7000C ZnO900^{0}C, and ZnO1100^{0}C are also shown in figure 6.6 [(a) – (d)] in which zinc and oxygen are the only detectable elements without any contamination. The variations of morphology at different temperatures are listed in table 6.1.

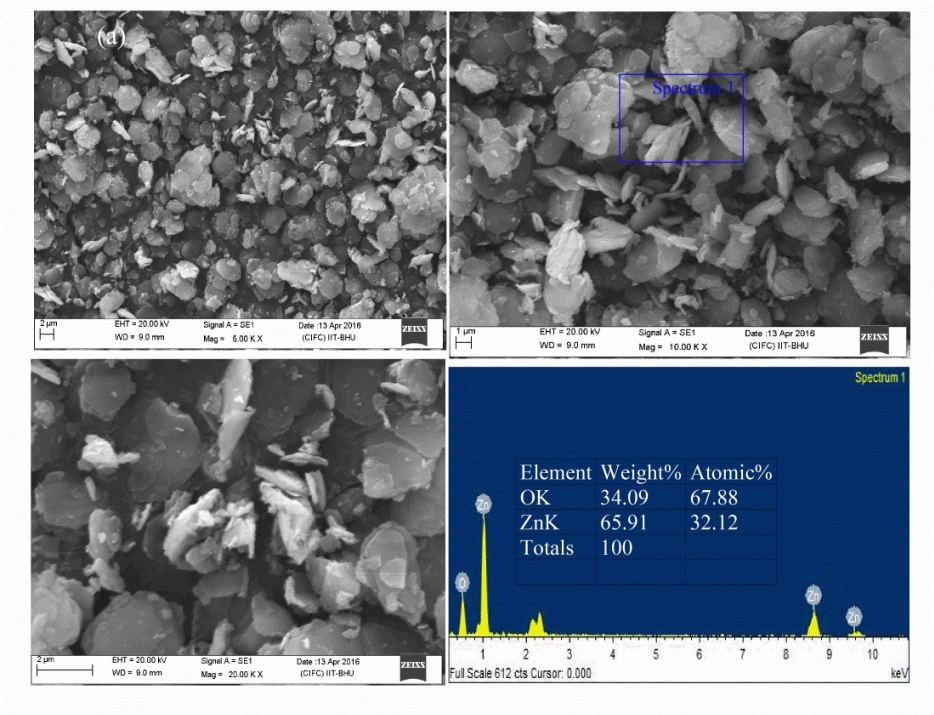

Figure6.6 (a) SEM image of sol-gel derived ZnO powder with increasing magnification and with EDX pattern.

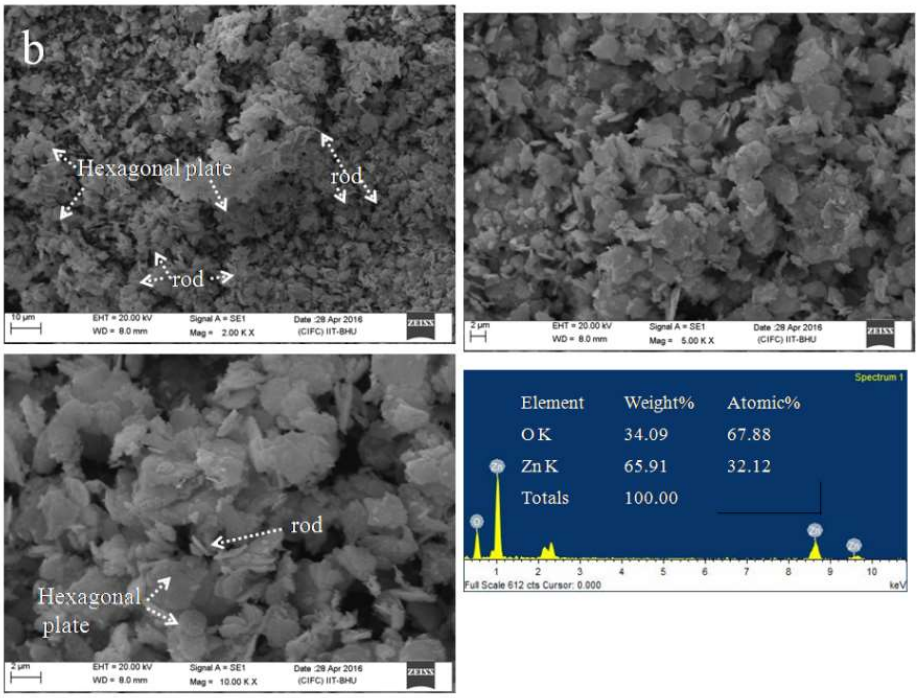

Figure 6.6(b) SEM image of ZnO700^{0}Cwith increasing magnification and with EDX pattern.

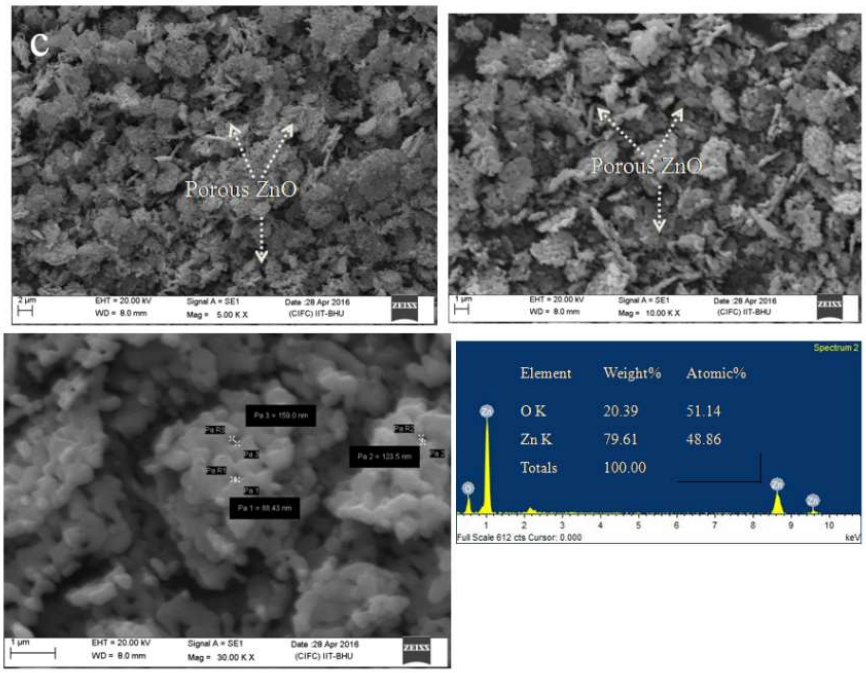

Figure 6.6(c) SEM image of ZnO900^{0}C with increasing magnification and with EDX pattern.

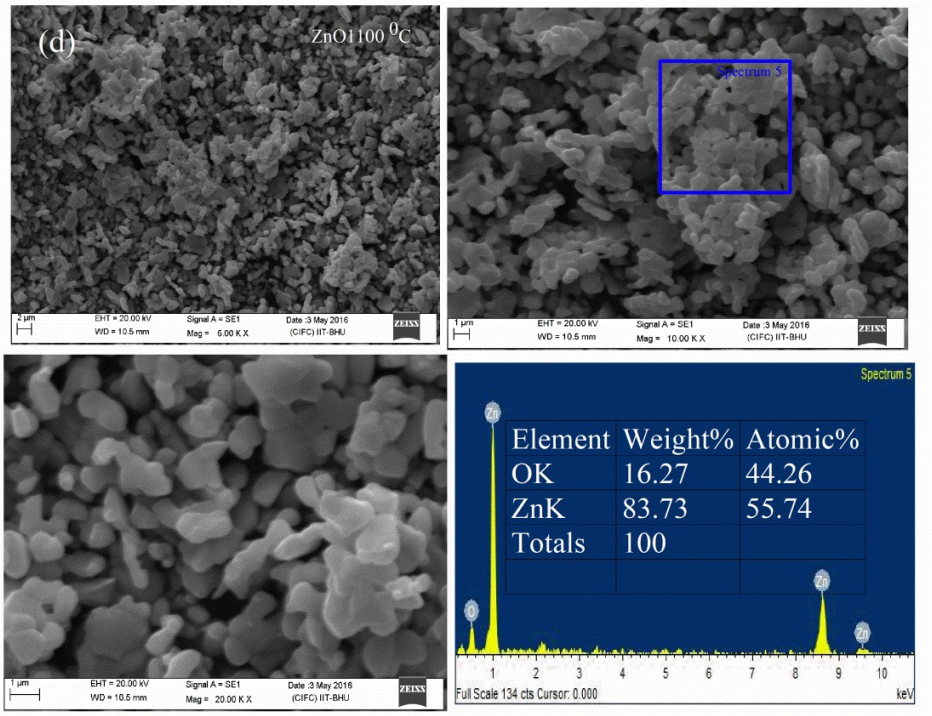

Figure 6.6(d) SEM image of ZnO1100^{0}C with increasing magnification and with EDX pattern.

6.2.6 HR-TEM and SAED analysis

Complementary morphological description can be achieved through the HR-TEM with the SAED study. Figure 6.6 (e), (f) shows the HR-TEM image of sample ZnO900. It is clearly shown from the image the particles are more or less in hexagonal plates shaped with a particle size distribution between 50-131nm.The average particles size has been calculated to be found 65nm shown in the bar graph. Figure6.6 (h) shows the selected area electron diffraction (SAED) pattern. The bright points in SEAD pattern show the crystalline nature whereas the ring pattern confirms the polycrystalline nature of the sample. From the figure6.6 [(I)-(L)] it is observed hexagonal plate-shaped ZnO particles are inter connected to each other as like chain and form a pore with a pore diameter in the range of 109-130nm (corner to corner).

At annealing temperature 900^0C the materials are impartment for practical application due to its porous structure and inter connection as chain-like structures.

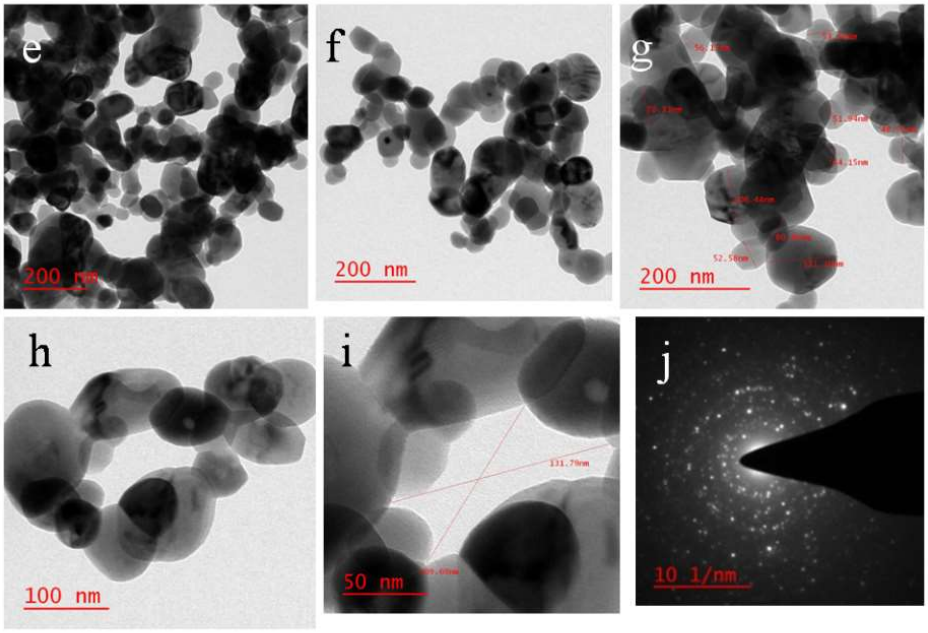

Figure6.6 (e, f) HR-TEM images of ZnO900^{0}C with increasing magnification, (g) Bar graph of ZnO900^{0}C, (h) SAED pattern of annealed ZnO900^{0}C.

6.2.7 FTIR analysis

Figure 6.7 shows that the FTIR spectrum of prepared ZnO and annealing at ZnO700^{0}C, ZnO900^{0}C, ZnO1100^{0}C present in the range 4000-400cm^{-1}. The peak between 3200cm^{-1} and 3600cm^{-1} shows the presence of hydroxyl (O-H) group with stretching vibrations of the –OH groups and deformation of the H-O-H band. In the sample ZnO900, the presence of hydroxyl groups are lower as compare to ZnO and Zn700 samples which is shown in figure 6.7 (b) and disappear in sample Zn1100 which indicates that increasing the annealing temperature the existing the water in zinc oxide is decreased. It is also observed that there is a negligible shift to a lower wave number due to an increase in the annealing temperature. This shift can be related to a change in the lattice parameters of ZnO. There were several absorption

bands at 1612 cm^{-1}, 1114 cm^{-1}, 1037 cm^{-1}.These absorption bands were likely related to CO_2 absorbed from the atmosphere (air) and can, therefore, be neglected. The peak at 460cm^{-1} is representing the sample having Zn-O bonds (Lepot N., et al. 2007).

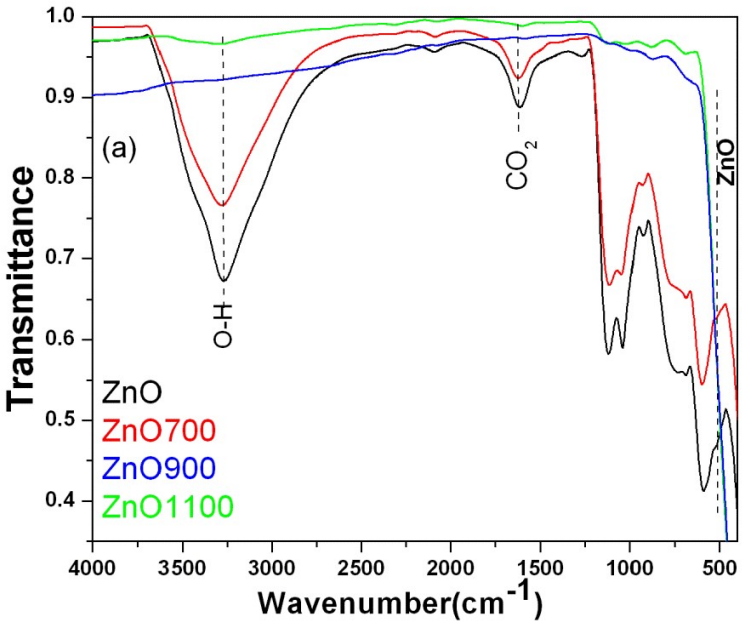

Figure 6.7(a) FTIR spectrum of prepared ZnO and annealing at ZnO700^{0}C, ZnO900^{0}C, ZnO1100^{0}C.

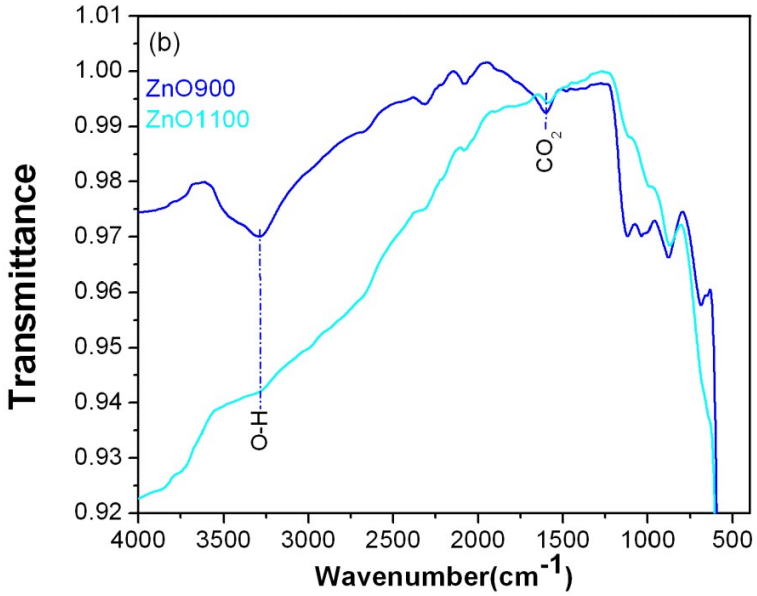

Figure 6.7 (b) FTIR spectrum of ZnO900^{0}C and ZnO1100^{0}C.

6.2.8 UV analysis

Figure6.8 [(a)-(c)] shows absorption of ZnO, ZnO700, ZnO900 and Zn1100. It was observed absorption of ZnO700 is lowered as compared to the ZnO and absorption of ZnO900 is lowered as compared to the ZnO1100.The relatively high value of absorption was observed in ZnO sample. In these, it is also observed the absorption spectrum shows a sharp absorbance at 345nm and represented by the dotted square, which indicates an almost uniform size of the nanoparticles. However, upon the change in particles size or particle shape, a slight shift in the wavelength was also observed, so annealing temperature has a pronounced effect on absorption and shape of ZnO nanoparticles. This behavior is due to the formation of smaller crystallites (Li Y. et al.2007), as also observed in XRD data [figure 6.1 (a)]. The inset of figure 6.8 (a) and figure 6.8 (b) shows the direct band gap of ZnO and ZnO700. Figure 6.8(d) and inset of figure 6.8 (d) shows the direct band gap of ZnO900 and ZnO1100.The direct band gap are estimated from the plot of $(\alpha h\upsilon)^2$ versus $h\upsilon$, where $h\upsilon$ is the photon energy and α is the ratio of the absorption coefficient to the scattering coefficient. From the figure the band gap was calculated and which are listed in table 6.1. From this table the crystallite size of RZ700 is smaller than other sample. Hence value of energy band gap (E_g) of RZ700 is more than other sample due to the quantum confinement effect (**Y.**Gu.et al.2004). It is also observed the band gap also slightly affected by increasing the annealing temperatures.

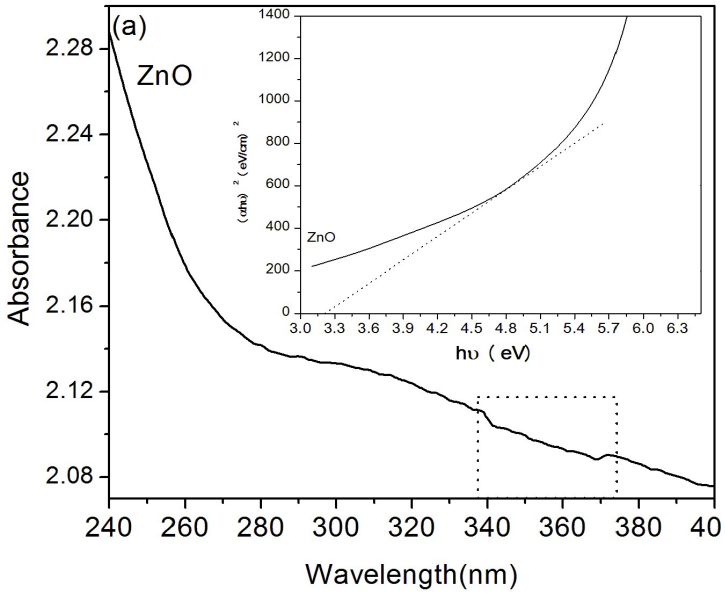

Figure 6.8 (a) UV-vis absorption spectra of ZnO and with their extracted optical band gap in the inset.

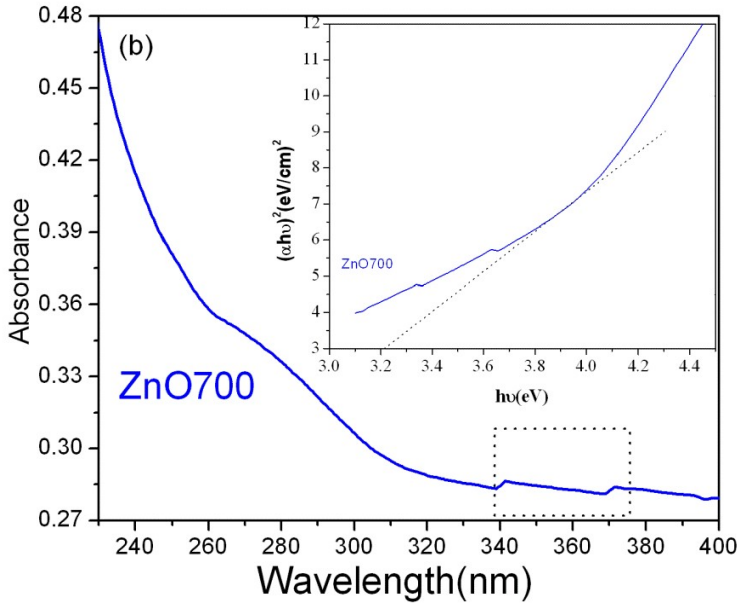

Figure 6.8(b) UV-vis absorption spectra of ZnO700^{0}C and with their extracted optical band gap in the inset.

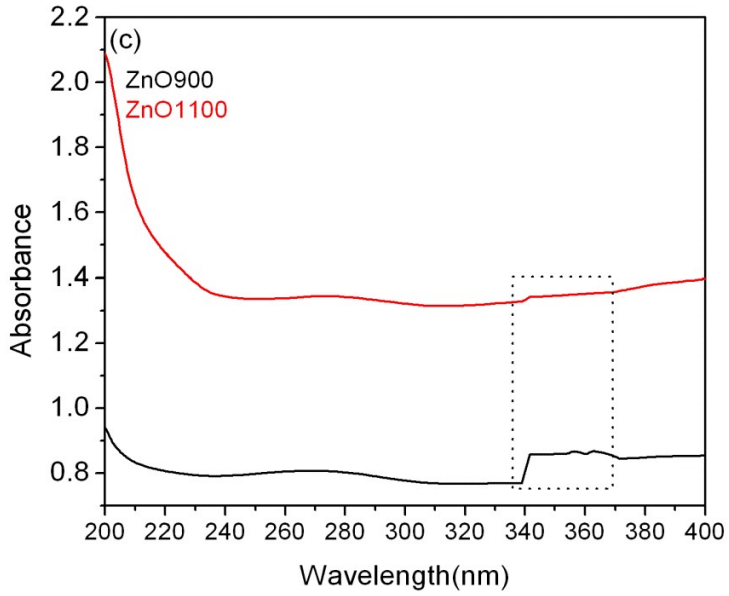

Figure6.8 (c) UV-vis absorption spectra of ZnOand with their extracted optical band gap in the inset.

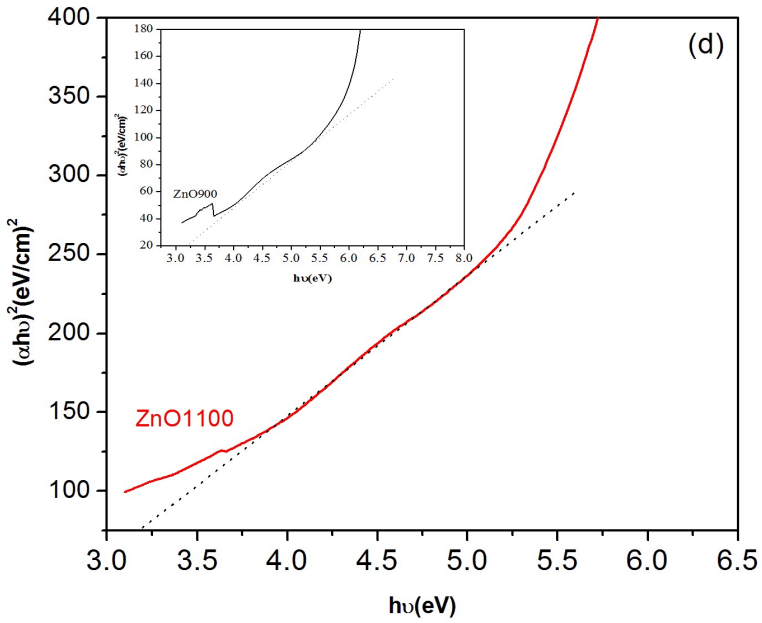

Figure 6.8 (d) UV-vis absorption spectra of ZnO900 and ZnO1100.

6.2.9 PL analysis

Figure 6.9 show two distinct sharp emission peaks at wavelengths 402nm and 426nm ZnO, ZnO700, ZnO900 and ZnO1100 respectively. The peak at 402 nm arises because of near-band-edge emission and a peak at 426nm arises due to the electronic transition. It is observed PL peak intensities at wavelengths 402nm and 426nm are increasing with increasing annealing temperature and maximum for the sample ZnO1100.The PL intensity increase significantly which may be due to the morphological variations of samples which are also depicted in SEM results. It is also observed that when annealing temperature increase the peaks are slightly shifted towards the higher wavelength this is due to variation of morphology with increasing temperatures.

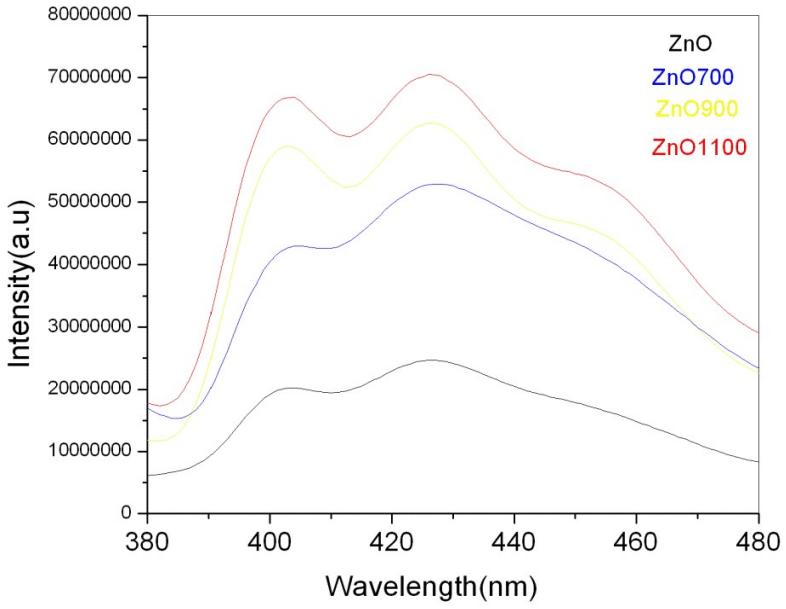

Figure6.9 PL spectra of ZnO, ZnO 700, ZnO900 and ZnO1100.

6.2.10 Dielectric Properties Analysis

Figure 6.10 [(a-d)] and its inset figure show the dielectric permittivity ε' and imaginary permittivity ε'' of ZnO sample as the function of frequency at different temperature. It is observed that dielectric constant below the low frequency 3.2 Hz shows step-like, this is due to containing the impurity and these behaviors are also seen in ε'' but does not show here. It is also observed that the value of ε' grows rapidly in the low-frequency region with increasing temperature. The higher values of dielectric constant observed at low frequencies region. The value of ε' at 75 ^{0}C, 175 ^{0}C and 200 ^{0}C are higher in the low-frequency region as compare to the temperature>200 ^{0}C. The values of ε'' also increase with increasing temperature in the low-frequency region which are shown in figure 6.11 [(a-d)] and in their inset figure. The increasing the value of ($\varepsilon', \varepsilon''$) in low-frequency region can be explained according to the behavior of grain boundaries at the interferences between the sample and the electrode, i.e., space charge polarization (K. R. Sambasiva,et al.2008) because of the dielectric permittivity related to free dipoles oscillating in the presence of an alternating electric field. At very low frequencies region ($f < 1/\tau$, τ is the relaxation time), dipoles follow the electric field. As the frequency increases, dipoles begin to lag behind the applied field at higher and higher frequencies (R. Ayouchi et al.2003) and ($\varepsilon', \varepsilon''$) decrease. When the frequencies reach the characteristic frequency ($f = 1/\tau$), the dielectric constant drops due to the relaxation process (R. Tripathi et al.2010). At very high frequencies ($f > 1/\tau$), dipoles can no longer follow the field (R. Tripathi et al.2010).

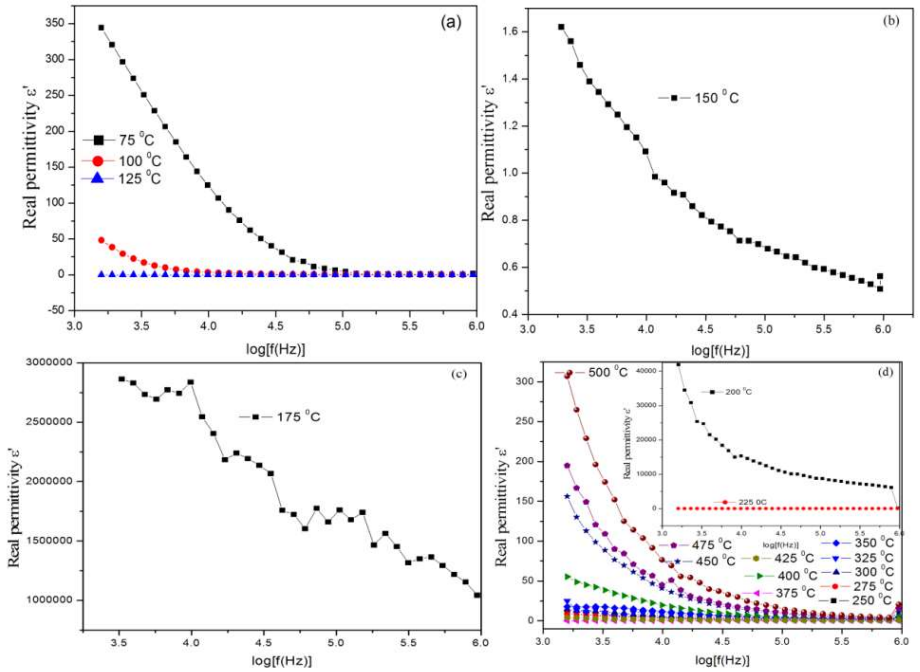

Figure 6.10 Variation of the real part of the dielectric constant of ZnO at temperature 75-125^{0}C (b) at temperature 150^{0}C (c) at temperature 175^{0}C (d) at temperature 200-225^{0}C in inset and at temperature 250-500^{0}C.

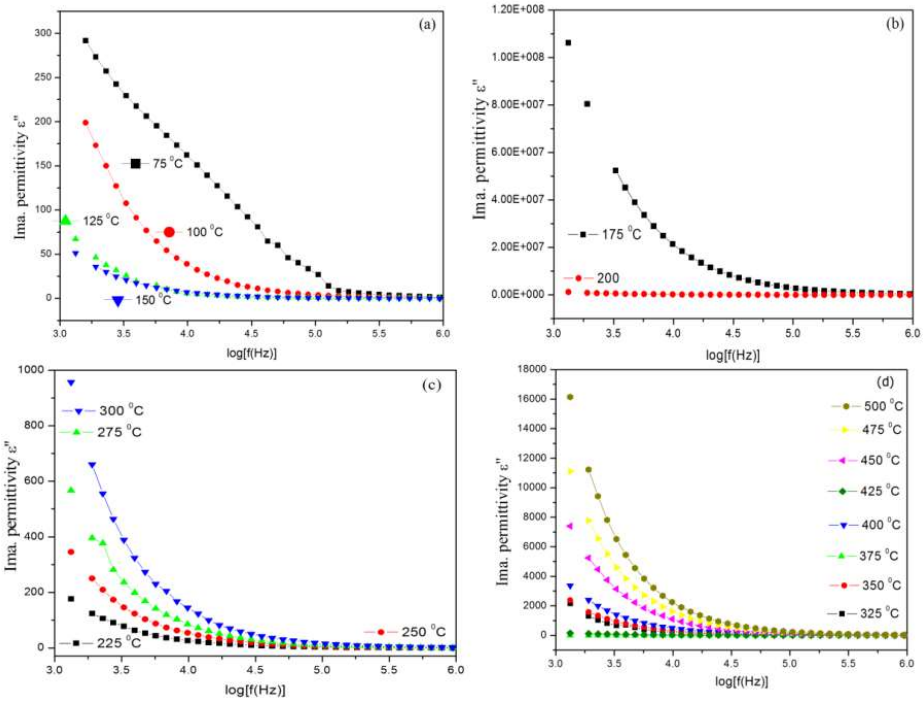

Figure6.11 Variation of the imaginary part of the dielectric constant of ZnO at temperature 75-150^{0}C (b) at temperature 175^{0}C (c) at temperature 225-300^{0}C (d) at temperature 325-500^{0}C.

Figure 6.12 (a), (b) and their inset figure show the dielectric permittivity ε' and imaginary permittivity ε'' of ZnO700 as the function of frequency. It is observed that dielectric constant ε' at temperature 75^{0}C and 100^{0}C shows step like but when temperatures increase its shows the value of ε' rapidly growing in the low-frequency region. It is also observed peak at temperature range 350^{0}C-400^{0}C with increasing ε' value in the low-frequency region which may represent relaxation peaks (R.Tripathi, et al.2010). These peaks occur when jumping frequency of localized electric charge carrier becomes approximately equal to that of the externally applied ac electric field (A.M. Abdeen, et al.2002). It is also observed the temperature >400^{0}C these peaks diapered which are shown in the inset of figure 6.12 (a). In this ε' are very close to each other below the temperature of 325^{0}C in the low-frequency region and some of

them merge to each other. This closeness is increase above the temperature of 325^{0}C. From the figure 6.12 (b) and inset of figure 6.12 (b) it is observed that values of ε" and closeness of the curves increase with increasing temperature in the low-frequency region. It is also observed that dielectric constant (ε', ε") decrease in the high-frequency region and it grows rapidly in the low-frequency region with increasing temperature due to space charge polarization (K. R. Sambasiva et al.2008).

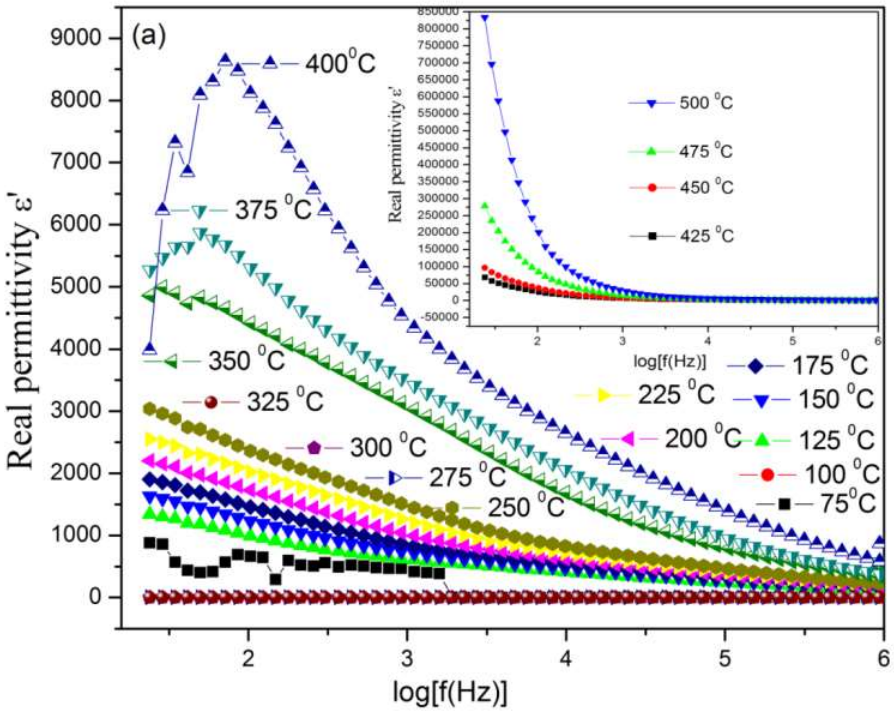

Figure 6.12 (a) Variation of the real part of the dielectric constant of ZnO700 at different temperature.

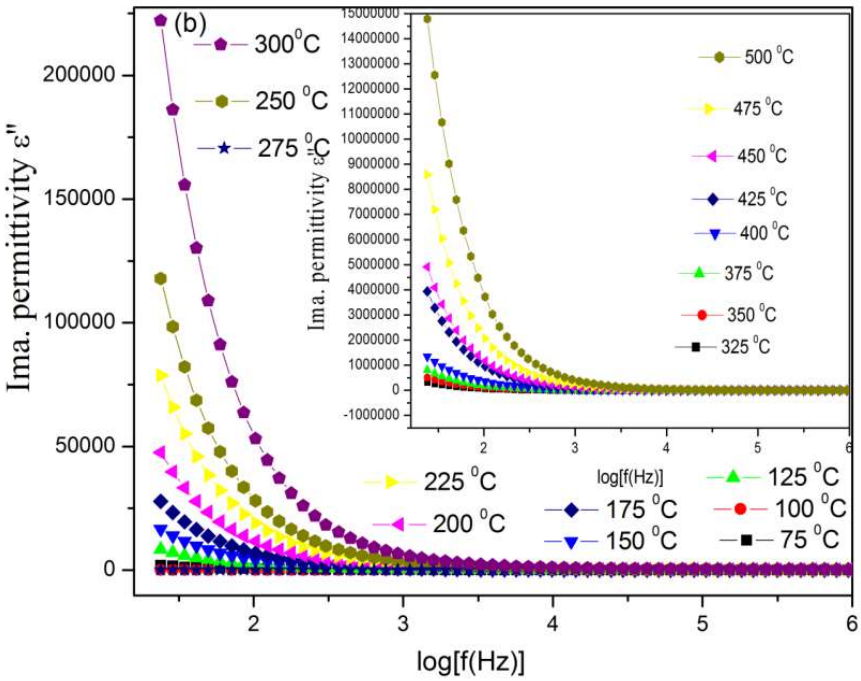

Figure 6.12 (b) Variation of the imaginary part of the dielectric constant of ZnO700 at different temperature.

Figure 6.13 (a), (b) and its inset show the dielectric permittivity ε' and imaginary permittivity ε'' of ZnO900 as the function of frequency at different temperature. It is observed that the value of ε' grows gradually in the low-frequency region with increasing temperature. It is also observed that the value of ε'' at temperature 75^0C-125^0C is higher in the high-frequency region as compared to the low-frequency region. In this figure value of ε'' at ~3 Hz are decreased with increasing temperature (<125 ^{0}C) and increasing below (>3 Hz) and above (<3 Hz) frequency region. In this figure relaxation peaks are observed in both low and high frequency region which is indicates relaxation process occurs in both high and low-frequency region due to structural morphology of ZnO900, whereas as increasing temperature (<325 ^{0}C) the relaxation peaks disappear and the value of ε'' increases

with increasing temperature in low-frequency region which is shown in inset figure of figure 6.13 (b). The relaxation peaks in the high-frequency region are also shifted toward the higher frequency with increasing temperature due to the increase hopping frequency of charge carriers between the metal ions (Kharabe R.G. et al.2006). So the ability of sample ZnO900 to be used frequency devices within the temperature range 150 ^{0}C$\leq T \leq$350^{0}C.

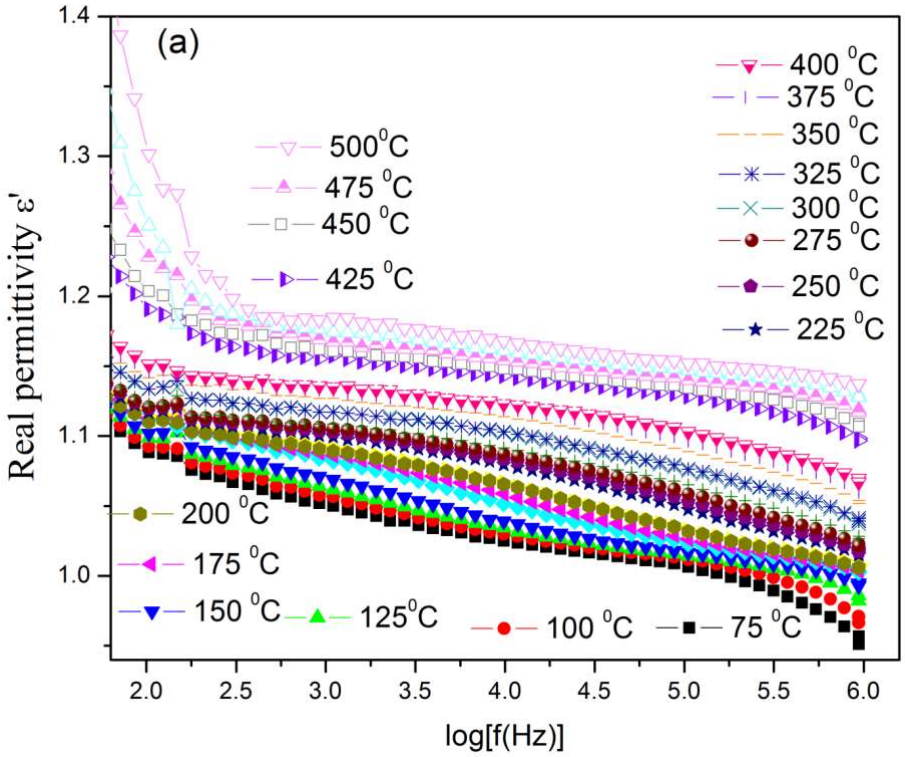

Figure 6.13 (a) Variation of the real part of the dielectric constant of ZnO900 at different temperature

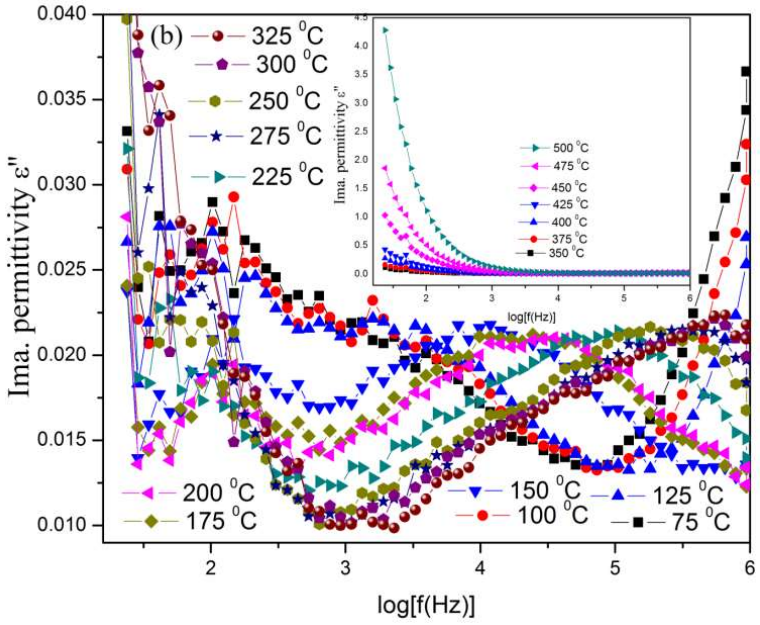

Figure 6.13 (b) Variation of the imaginary part of the dielectric constant of ZnO900 at various temperatures.

Figure 6.14 [(a-d),(e-h)] and its inset show the dielectric permittivity ε' and imaginary permittivity ε'' of ZnO1100 as the function of frequency with increasing temperatures. Figure 6.14 (a) shows the value of ε' at temperature 100^0C-150^0C is increasing in low-frequency region and also observed relaxation peaks in the low-frequency region whereas at temperature 125^0C slightly increase in the high-frequency region. Figure 6.14 (b) and inset figure show the value of ε' is an increase in the low-frequency region. Figure 6.14 (c) and inset figure show the value of ε' are an increase in the low-frequency region and also observed a relaxation peak in this region. In this figure, it is also observed relaxation peak in the low and high-frequency region at temperature 250^0C which indicates relaxation process occurs both high and low-frequency region at this temperature. Figure6.14 (d) and inset figure show the value of ε' are an increase in low-frequency region due to dipole moment. Figure 6.14 [(a-d)] it is observed that the value of ε' is an increase in low-

frequency region with increasing the temperature whereas at temperature 175^{0}C and 200^{0}C are decreasing and also observed relaxation peaks in low-frequency regions. Figure6.14 [(e-h)] and its inset figure show the value of imaginary permittivity ε" of ZnO sample as the function of frequency at different temperature. It is observed the values of the ε"are an increase in low-frequency region with increasing the temperatures. Increasing and decreasing behavior of (ε',ε") in this figure due to space charge polarization (K. R. Sambasiva,et al.2008).

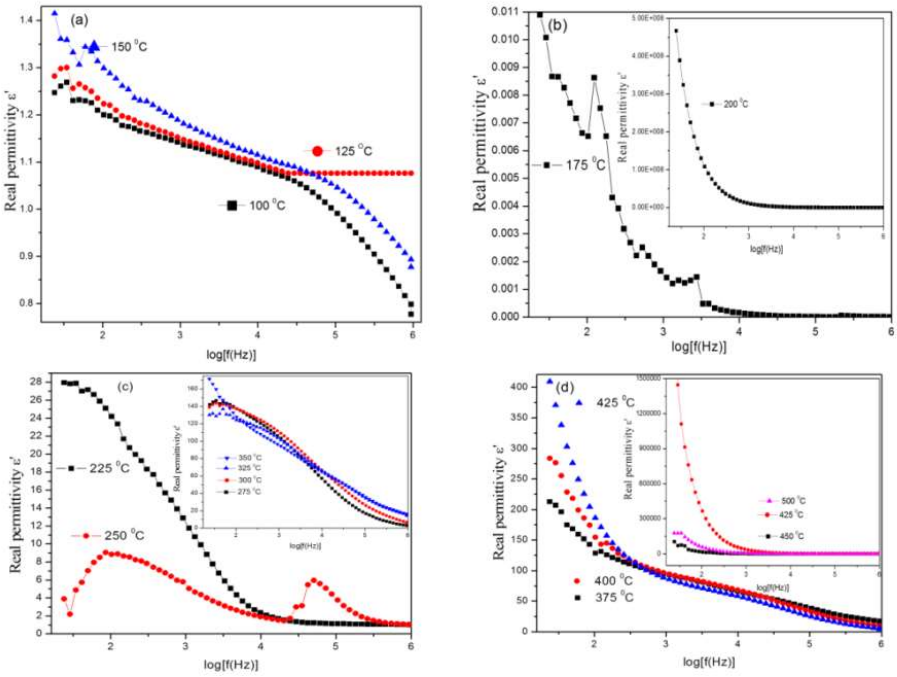

Figure6.14 (a) Variation of the real part of the dielectric constant of ZnO1100 at temperature 100-150^{0}C (b) at temperature 175^{0}C and inset at 200 ^{0}C,(c) at temperature 225^{0}C, 250^{0}C and inset at temperature 275- 350^{0}C,(d) at temperature 375-425^{0}C and inset at 450- 500^{0}C.

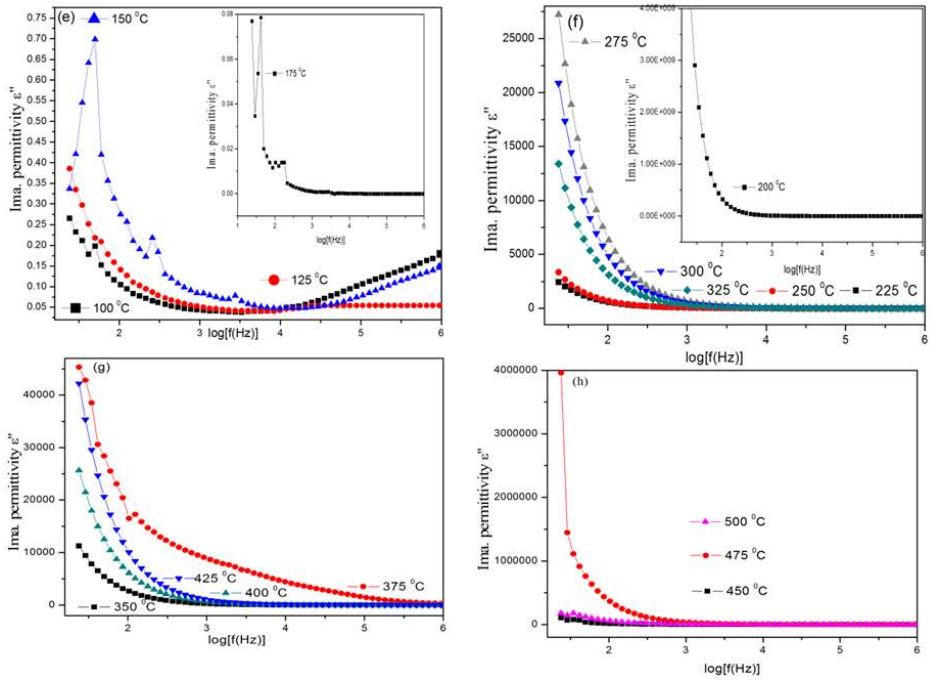

Figure 6.14 (e) Variation of the imaginary part of the dielectric constant of ZnO1100 at temperature 100-150^{0}C and inset at temperature 175^{0}C (f) Inset at temperature 200^{0}C and at temperature 225-325^{0}C, (g) at temperature 350-400^{0}C (h) at temperature 450-500^{0}C.

We can conclude the all samplesZnO,ZnO700,ZnO900, and ZnO1100) are found to exhibit the dielectric dispersion where the dielectric constants (ε',ε'') decrease as frequency increases and the higher values of dielectric constant, observed at low frequencies region this is due to space charge polarization in inhomogeneous dielectric structure (K. R. Sambasiva et al.2008) because the homogeneities present in the sample ZnO are hexagonal plate, in the sample ZnO700 are rod and disk, in the sample ZnO900 are porous like structure and in the sample ZnO1100 are grain-like structures which are depicted in SEM results. Again the next point comes into picture from all the above figure is the temperature dependence of dielectric constant. In general ε' and ε'' increases as the temperature increases indicating the

semiconducting nature of ZnO. The dielectric dispersion of (ε',ε'') is weak in the low-temperature region. With the increasing temperature, it increases shapely in the low-frequency region whereas in sample ZnO900 this behavior observed both in the low and high-frequency region for ε''. This effect may be due to the porosity structure of ZnO. It can be explained on the basis that at relatively low temperature, the charge carries on most cases cannot orient themselves with respect to the direction of the applied field, therefore; they possess a weak contribution to the polarization and affected the dielectric behavior. As the temperature increases, the charge carriers get enough excitation thermal energy to be able to obey the change in the external field more easily. These thermal excitations of atoms about their lattice points may be due to disorder at the lattice. Space charge contribution to the polarization may be attributed to the purity of the crystal; this in return enhances their contribution to the polarization leading to an increase of dielectric behavior.

Further, it is also clear from Figure 6.10[(a-d)], Figure 6.12(a), Figure 6.13(a), and Figure 6.14(a-d), show that the dielectric constant (ε',ε'') also dependent on the structure of the sample. The dielectric constant ε' for ZnO700 show relaxation peaks at temperature 350 ^{0}C-400^{0}C and for ZnO1100 at temperature 100^{0}C-350 ^{0}C in low-frequency region while this behavior mostly disappears for the sample ZnO and ZnO900. This characteristic is dielectric anomaly referred to as the temperature dependence of the dielectric permittivity at given frequencies. On the other hand, the elevation of temperature facilitates which is a benefit to the dipole polarization at low frequency and thus dielectric permittivity is improved.

6.2.11 Ac conductivity analysis

Figure 6.15 (a-d) shows the frequency dependence of Ac conductivity (σ) of ZnO, ZnO700, ZnO900 and ZnO1100 respectively at a different temperature which is calculated by eqn (3.31). The conductivity-frequency dependent spectra divided into three regions and represented by a solid line which is shown in figure 6.15 [(a-d)]. In the region (I) the conductance approximately equal to dc value (σ_{dc}).The region (II&III) represent the dispersive region. For the dispersive region, it is observed that conductivity increase with increase as the frequency of applied ac field increase. With increasing frequency conductive spectra becomes more dispersive. It is also observed values of conductivity also increase with increasing the temperature due to hopping of charges for conduction. Figure 6.15 (a) the frequency conductive spectra dispersive region at temperature 325^0C and 375^0C exhibits multiple step-like increments which is characteristics of potential profile with multiple activation energies (F. Barsoukov, et al.2005). The highest conductivity is observed in the sample ZnO700 and lowest value of conductivity observed in the sample ZnO900. In All figure 6.15 [(a-d)] curves show the conductivity in low-frequency region almost constant value assigned the dc conductivity for the grain boundaries (σ_{gb}) which is refers the Schottky barrier height at the σ_{gb} and frequency independent plateau in the II region is due to dc conductivity for the grains (σ_g). This behavior is a strong dependence on the frequency owing to their insulating nature. This result is in good agreement with the variation of dielectric properties of the ZnO samples. It is also absorved at higher frequency region relaxation polarization is submerged by the hopping-like conductivity. In the equation (3.31) the values of σ_{dc}, ω_H and n are

obtained by the fitting of the frequency dependent conductivity $\sigma'(\omega)$ data measured experimentally at different temperatures for the different frequency regions. The increase in σ_{ac} with the applied frequency can be explained on the basis that the pumping force of the applied frequency that helps in transferring in the charge carriers between the different localized states as well as liberating the trapping centers. These charge carriers participate in the conduction process simultaneously with electrons produced from the valance exchange between the metal ions (Y. Li et al. 2007). However, as frequency increases the conductivity becomes more and more frequency dependent. The very basic fact ac conductivity is increased with increasing the temperature due to the increase in drift mobility of the thermally activated charge carriers (M.A. Ahmed et al.1995).

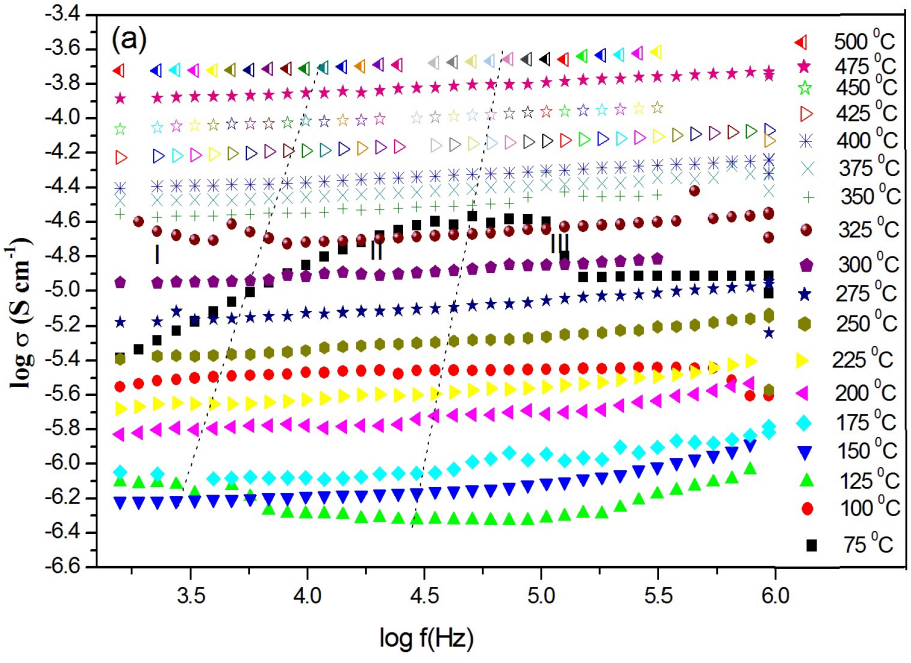

Figure 6.15(a) Variation conductivity at different temperature of ZnO.

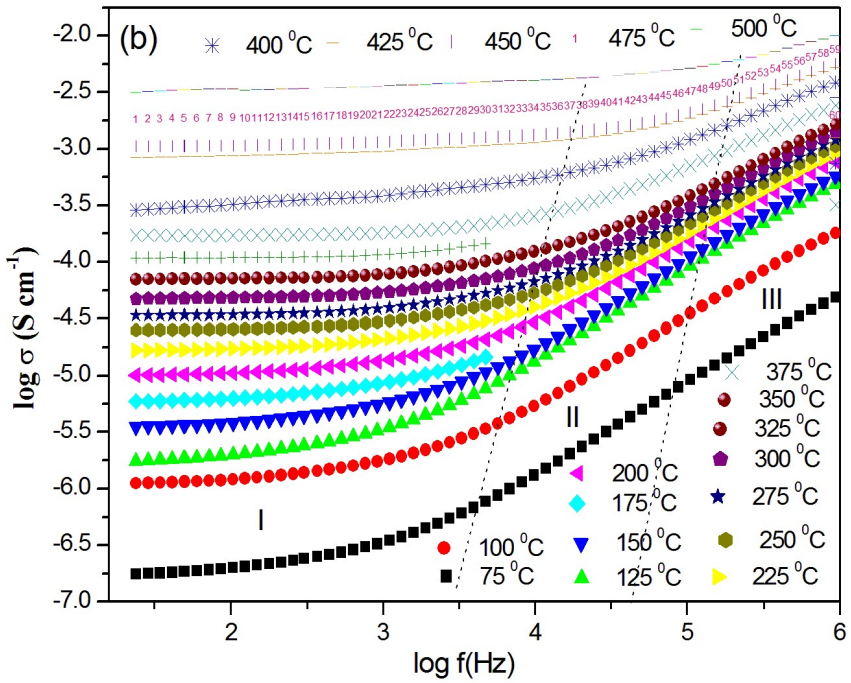

Figure 6.15(b) Variation conductivity at different temperature of ZnO700.

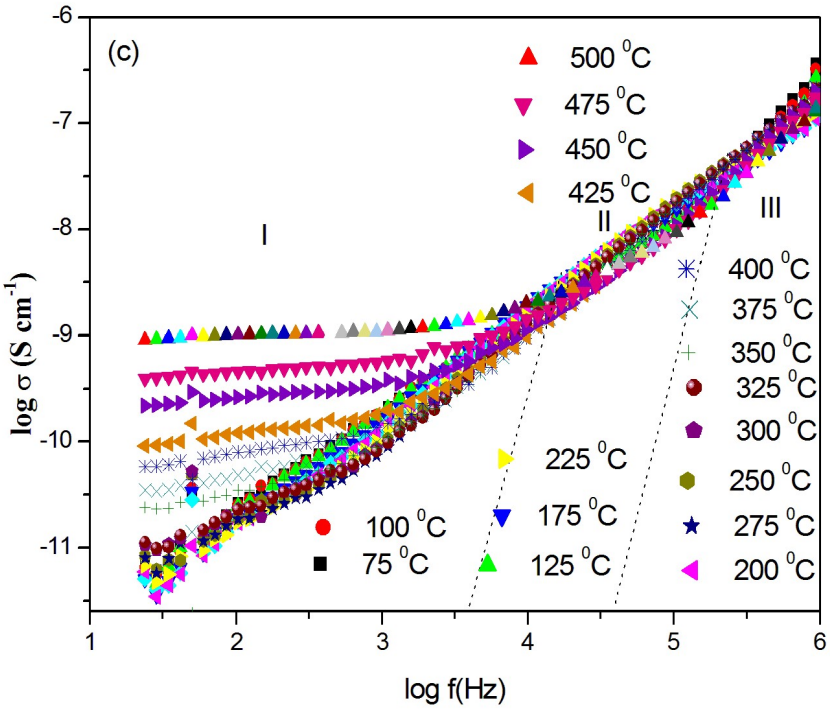

Figure 6.15(c) Variation conductivity at different temperature of ZnO900.

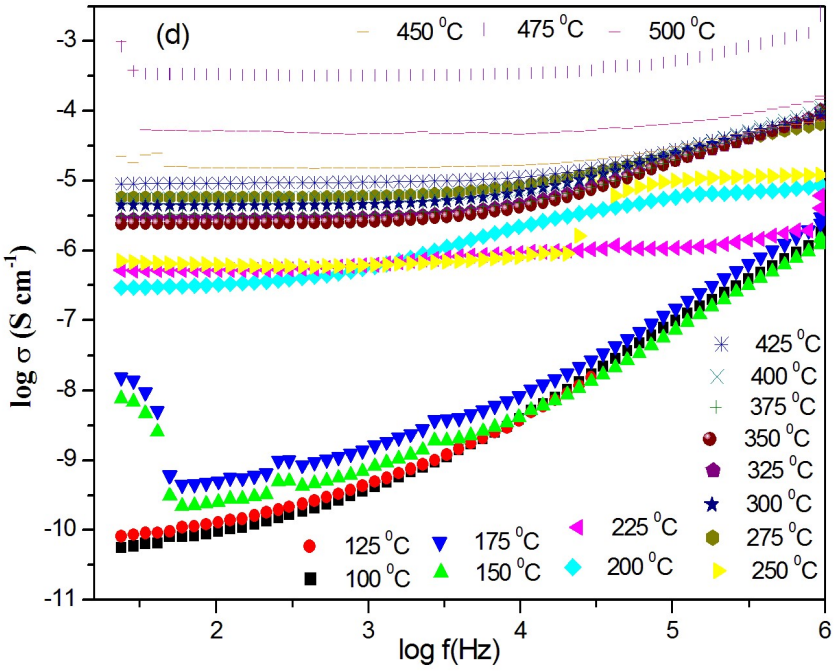

Figure 6.15(d) Variation conductivity at different temperature of ZnO1100.

Summary of Results

It is conclude that the hexagonal plate-shaped Zinc oxide structure was successfully synthesized by the sol-gel method.The effect of different annealing temperature 700^0C, 900^0C, and 1100^0C on the hexagonal plate like morphology with constant heating rate has been investigated by characterization technique. Real and imaginary part of the dielectric constant was found to effect by annealing temperature and increase with increasing temperature and found to decrease with increasing frequency. Variation of dielectric properties is observed due to the changes of space charges/interfacial polarization resulting from the variations of surface to volume ratio of nanomorphology. Real and imaginary part of the dielectric constant was found to effect by annealing temperature and increase with increasing temperature and found to decrease with increasing frequency. Dielectric content (D.C) of ZnO700 (rod and disk) is higher value as compare to the other resultant morphology.